Effect of Hot Body Noise Sources on Arrays of Deep Space Network Antennas

Marc Sanchez Net*

ABSTRACT. — This article provides a model to estimate the effect of hot body noise on arrays of Deep Space Network (DSN) antennas using principles of communications systems and microwave radiometry. It provides approximations to calculate the increase in system noise temperature (or reduction in gain-to-noise-temperature ratio [G/T]) when the array tracks a spacecraft close to a source of microwave radiation. Through this analysis, we show that the array performance is not only driven by the main lobe of the array's radiation pattern but also by grating lobes characteristic of arrays of widely separated elements.

Using this model, we provide a way to classify sources of hot body noise as extended or compact and provide simplified expressions for the array performance in the case of very extended and very compact sources. We provide several numerical examples, including the noise temperature induced by Jupiter during a Juno flyby when the spacecraft was tracked by an array of three DSN 34-m beam waveguide antennas operating at X- and Ka-band.

I. Introduction

NASA's Deep Space Network (DSN) operates 14 antennas across three sites in Goldstone, California, Madrid, Spain, and Canberra, Australia. Each complex is equipped with one 70-m antenna, four or five 34-m antennas, and a signal processing center [1]. They are used routinely to track ∼40 spacecraft and provide services such as commanding, telemetry, and tracking.

To increase downlink performance, the signal processing electronics at each complex include two correlators that can array multiple antennas [1]. Operational tracks in this

*Communications Architectures and Research Section.

The research described in this publication was carried out by the Jet Propulsion Laboratory, California Institute of Technology, under a contract with the National Aeronautics and Space Administration.

arrayed configuration have been performed at S- and X-band for several years. More recently, operation of the array at Ka-band has been suggested as a way to increase data rates at outer planet distances.

This article summarizes research conducted at the Jet Propulsion Laboratory (JPL) to quantify the effect of planetary noise on an array of DSN antennas at multiple frequency bands, including Ka-band. It provides an analytical framework to derive exact and approximated equations for quantifying the increase in system noise temperature when the array is used to track a spacecraft flying close to a source of hot body noise (e.g., a planet). The problem formulation follows the reasoning from Reference [2] but uses the well-known concept of the *array factor* (e.g., Reference [3]) to estimate the equivalent noise temperature of the hot body source as seen by the entire array. Compared to Reference [2], it also converts units and terms from conventions used in astronomy to equivalent concepts used in the communications literature.

This article is structured as follows: The rest of Section I discusses the system model and outlines the assumptions used in the rest of the document. Section II discusses the operation of a single DSN antenna when tracking a spacecraft close to hot body source and derives expressions for its signal-to-noise ratio (SNR) and G/T. Section III extends the analysis to a possibly heterogeneous array of DSN antennas. Next, Section IV provides simplified equations to classify noise sources as extended or compact, and derives limiting expressions on array performance under both conditions. Finally, Section V uses the equations derived in previous sections to estimate the performance of an array of 34-m antennas tracking Juno during a flyby at both X- and Ka-band.

A. System Model

We consider a single spacecraft communicating with the DSN in the downlink direction. The spacecraft is orbiting or flying by a solar system body (which is assumed to be a planet for simplicity) that degrades the system performance because it is a source of broadband hot body noise. Additionally, each antenna experiences thermal noise due to Earth's atmosphere, microwave electronics, and background galactic radiation.

Figure 1 provides a graphical representation of the system under consideration and depicts three DSN 34-m beam waveguide (BWG) antennas tracking a spacecraft orbiting a planetary body.[1] The antennas are assumed to operate in array mode, and are phased to maximize the SNR of the signal received from the spacecraft, while the planet acts as a source of noise. The process by which this phasing occurs is not discussed in this article; the reader is instead directed to previous publications such as Reference [4]. Furthermore, we assume for the sake of simplicity that:

[1] For the sake of clarity, Figure 1 only shows three antennas. However, the formulation and analysis presented in subsequent sections of this article assume a general array of N antennas.

- The hot body noise does not introduce large errors in the phasing process, which would significantly distort the array factor.
- The effect of atmospheric losses is obviated. In general, they attenuate the received signal, reducing the array SNR, but also attenuate the hot body noise arriving from the planetary body.

Consequently, the expressions for array SNR and G/T provided in the article should be interpreted as approximations for the achievable system performance.

Because of the large distances between transmitter and receiver, we assume that at any given point in time the spacecraft can be modeled as a point source defined by its position (θ_0, φ_0) in the local sky, expressed in spherical coordinates. Similarly, the planetary body radiation arrives to the antennas from all directions within a solid angle Ω_p, which depends on the diameter of the planetary body and its distance to Earth. Both (θ_0, φ_0) and Ω_p are assumed to be equal for all antennas in the array because the baselines are orders of magnitude smaller than the planetary distance.

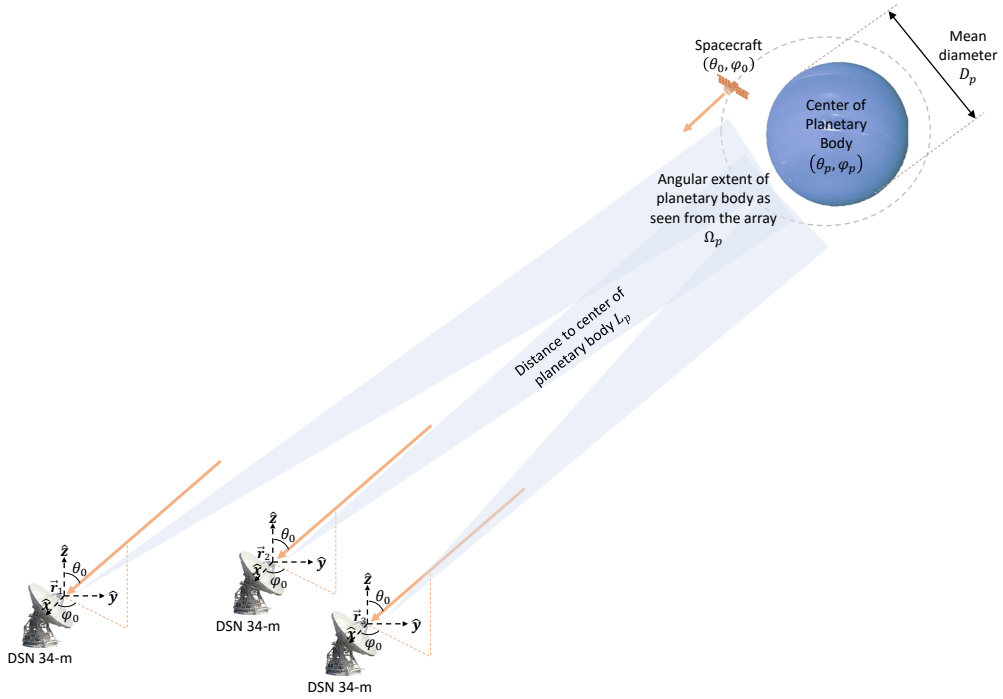

Figure 1. DSN array with three 34-m BWG antennas.

Let $\vec{\mathbf{r}}_i(t)$ denote the position of the i-th antenna in the array[2] and let $\vec{\mathbf{r}}_0(t)$ denote the position of the spacecraft. The delay experienced by the wavefront traveling from the

[2]This position is associated with a reference point in the antenna, usually the intersection of the azimuth and elevation axes.

spacecraft to the i-th antenna, assuming free space propagation and no atmospheric or relativistic effects, is given by

$$\tau_i(t_T, t_{R_i}) = \frac{|\vec{\mathbf{r}}_i(t_{R_i}) - \vec{\mathbf{r}}_0(t_T)|}{c}, \tag{1}$$

where c is the speed of light, t_T is the time of the departure of the signal from the spacecraft, and t_{R_i} is the time of arrival at the i-th antenna. This expression can be simplified using the well-known far-field approximation [3], which is always valid at planetary distances. In particular,

$$\begin{aligned}
\tau_i(t_T, t_{R_i}) =& \frac{1}{c}\sqrt{r_0^2 + r_i^2 - 2r_0 r_i \hat{\mathbf{r}}_i \cdot \hat{\mathbf{r}}_0} \\
=& \frac{r_0}{c}\sqrt{1 + \frac{r_i}{r_0}\left(\frac{r_i}{r_0} - 2\hat{\mathbf{r}}_i \cdot \hat{\mathbf{r}}_0\right)} \\
\approx& \frac{r_0}{c}\left[1 + \frac{1}{2}\frac{r_i}{r_0}\left(\frac{r_i}{r_0} - 2\hat{\mathbf{r}}_i \cdot \hat{\mathbf{r}}_0\right) + \mathcal{O}\left(\tfrac{r_i^2}{r_0^2}\right)\right] \\
\approx& \frac{r_0}{c}\left[1 - \frac{r_i}{r_0}\hat{\mathbf{r}}_i \cdot \hat{\mathbf{r}}_0\right] \\
=& \frac{r_0(t_T)}{c} - \frac{\vec{\mathbf{r}}_i(t_{R_i}) \cdot \hat{\mathbf{r}}_0(t_T)}{c},
\end{aligned} \tag{2}$$

where

- we have used the notation $|\vec{\mathbf{a}}| = a$;
- we have removed the time dependency everywhere except in the final line of the derivation to ease notation;
- we have used the fact $\sqrt{1+x} \approx 1 + \frac{x}{2}$ when $x \ll 1$;
- we have used the fact that $\frac{r_i}{r_0} \ll 1$ to neglect all terms of second order or higher;

As noted later in this article, the performance of the array depends on the difference in propagation delay between the signals arriving at each of the array elements. Using Equation (2), this difference can be approximated as

$$\begin{aligned}
\tau_i(t_T, t_{R_i}) - \tau_j(t_T, t_{R_j}) \approx& -\frac{\left[\vec{\mathbf{r}}_i(t_{R_i}) - \vec{\mathbf{r}}_j(t_{R_j})\right] \cdot \hat{\mathbf{r}}_0(t_T)}{c} \\
\approx& -\frac{\left[\vec{\mathbf{r}}_i(t_R) - \vec{\mathbf{r}}_j(t_R)\right] \cdot \hat{\mathbf{r}}_0(t_T)}{c} \\
=& \frac{\vec{\mathbf{B}}_{ji} \cdot \hat{\mathbf{r}}_0(t_T)}{c},
\end{aligned} \tag{3}$$

where the second approximation follows from ignoring the change in position due to planetary motion between the time of arrival of the wavefront at the two antennas, and $\vec{\mathbf{B}}_{ji}(t) = \vec{\mathbf{r}}_j(t) - \vec{\mathbf{r}}_i(t) = -\vec{\mathbf{B}}_{ij}(t)$ is defined as the baseline between the j-th and i-th antenna, which is constant in time because we assume the antennas are fixed to the ground.

B. Assumptions

Given the geometry of Figure 1, we make the following assumptions:

(A.1) Without loss of generality, all calculations are performed on a topocentric reference frame fixed on one of the antennas in the array (or a reference point close to all of them). They are expressed in spherical coordinates using the following convention: θ is the zenith angle (also known as colatitude) and φ is the azimuthal angle. The solid angle $\Omega = (\theta, \varphi)$, expressed in steradian, defines the field of view of an object in the sky as seen by the antennas and has differential, in spherical coordinates,

$$d\Omega = \sin\theta d\theta d\varphi. \tag{4}$$

(A.2) The spacecraft is assumed to operate close to a planetary body that emits electromagnetic (EM) radiation at the frequency band of interest. For directive antennas, "close to" is understood to mean approximately that the primary lobe of the antenna intersects with the planetary disk. However, our formulation is general and makes no use of this fact.

(A.3) The spacecraft transmits a narrowband signal $s(t)$ that is assumed to (1) be fully contained in a bandwidth B, (2) be wide-sense stationary, (3) have constant power normalized to unity, and (4) be uncorrelated during a time interval $\mathcal{T}$. Mathematically,

$$R_s(t-t') = \langle s(t)s^*(t')\rangle_{\mathcal{T}} = \begin{cases} 1 & \text{if } t-t'=0 \\ 0 & \text{if otherwise,} \end{cases} \tag{5}$$

where $\langle\cdot\rangle_{\mathcal{T}}$ denotes the time-average over an integration interval of $\mathcal{T}$ seconds.

(A.4) The spacecraft telecommunications subsystem is capable to producing P_t watts of radio frequency (RF) power at the desired frequency band. It also includes an antenna with gain G_t such that the power flux density, in $\frac{W}{m^2}$, at a distance R and assuming free space propagation and no losses is

$$S_{sc} = \frac{P_t G_t}{4\pi R^2}. \tag{6}$$

(A.5) The spacecraft is assumed to be a point source located at (θ_0, φ_0) in the sky, as seen from the DSN stations. The electric field received by the DSN station, in $\frac{V}{m}$, is modeled as

$$E_{sc}(t, \theta, \varphi) = \sqrt{S_{sc}}s(t)\delta(\theta - \theta_0, \varphi - \varphi_0), \tag{7}$$

where $\delta(\cdot)$ denotes the Dirac-delta function. Note that Equation (7) neglects the propagation delay because t, as defined in Assumption (A.2), is the instant of

time associated with the departure of the signal from the spacecraft. This is acceptable because the system performance only depends on the relative delays between the front ends of $E_{sc}(t)$ at each antenna in the array.

(A.6) Losses due to non-ideal factors (e.g., implementation losses at the transmitter or receiver, atmospheric losses) are neglected in the analysis. They are assumed to affect the system equally whether operating using a single antenna or an array.

(A.7) The planetary body emits broadband spatially and temporally uncorrelated radiation according to the laws of microwave radiometry. In other words, the electric field $E_p(t,\theta,\varphi)$ from the planetary body at a given frequency f at the receiving antenna satisfies

$$\langle E_p(t,\theta,\varphi)E_p^*(t',\theta',\varphi')\rangle_\tau = \begin{cases} I_p\left(f,\theta,\varphi\right) & \text{if } \ t=t' \text{ and } (\theta,\varphi)=(\theta',\varphi') \\ 0 & \text{otherwise,} \end{cases} \tag{8}$$

where $I_p\left(f,\theta,\varphi\right)$ is the spectral brightness intensity of the planet, measured in $\frac{W}{m^2 sr Hz}$. This spectral brightness intensity is assumed to be constant and vary slowly with frequency, and is estimated in accordance to Planck's law.

(A.8) The system is assumed to operate at Ka-band or below. Therefore, the Rayleigh-Jeans approximation for the spectral brightness intensity is assumed to be valid so that

$$I_p\left(f,\theta,\varphi\right) \approx \frac{2k}{\lambda^2} T_b\left(\theta,\varphi\right), \tag{9}$$

where k denotes the Boltzmann constant, $T_b\left(\theta,\varphi\right)$ is the brightness temperature of the planet, which need not be constant over the entire body, and λ is the wavelength of operation. Note that $I_p\left(f,\theta,\varphi\right)$ provides the flux of *unpolarized* radiation per unit of solid angle and frequency.

(A.9) Each DSN antenna in the array is modeled using its effective aperture $A\left(\theta,\varphi\right)$, which is known to be related to the antenna gain by

$$A\left(\theta,\varphi\right) = \frac{\lambda^2}{4\pi} G\left(\theta,\varphi\right). \tag{10}$$

Using this definition, the differential of power (in watts) intercepted by the antenna from a (differential) source at coordinates (θ,φ) in the local sky, and delivered to a matched load connected to the antenna, is equal to

$$dP_{rx}(\theta,\varphi) = S_{sc} dA\left(\theta,\varphi\right) = S_{sc} A_e F(\theta,\varphi) d\Omega, \tag{11}$$

where $A_e = \frac{\lambda^2}{4\pi} G_{max}$, G_{max} is the peak gain of the antenna, and $F(\theta,\varphi)$ is the normalized radiation pattern such that $\max\limits_{(\theta,\varphi)} F(\theta,\varphi) = 1$. This can be equivalently expressed as

$$dP_{rx}(\theta,\varphi) = \frac{P_t G_t}{L} G(\theta,\varphi) d\Omega, \tag{12}$$

where $L = \left(\frac{4\pi R}{\lambda}\right)^2$ is the well-known free space loss of the Friis transmission equation (also known as link budget).

(A.10) All antennas are assumed to be perfectly pointed towards the spacecraft, which is located at coordinates (θ_0, φ_0). No pointing losses or pointing errors are considered.

(A.11) All antennas are assumed to be equipped with microwave electronics with a known and quantifiable equivalent noise temperature. They also "see" noise from external sources, such as the Earth's atmosphere or the galactic cosmic radiation. All these sources of thermal noise (excluding the planetary body) are lumped into a single parameter, the equivalent thermal noise temperature, which is denoted by T_n. It generates additive white Gaussian noise (AWGN) with power equal to kT_nB watts, *per polarization*.

(A.12) The spacecraft, planet, and thermal noise are assumed to be independent and uncorrelated sources of electric field.

Using the system model from Figure 1, as well as the Assumptions (A.1)–(A.12), we now proceed to derive the system SNR and G/T when the spacecraft is tracked by a single DSN antenna or an array of antennas. In each case, we first derive the power of the signal received from the spacecraft and the thermal noise. Then we quantify the additional noise power contribution from the planetary body.

II. Analysis for a Single Antenna

A. Spacecraft Signal Power

The voltage (measured in volts) at the output of the DSN antenna is equal to

$$v_{sc}(t) = \sqrt{A_e} \iint\limits_{\Omega_{sc}} \sqrt{F(\theta,\varphi)} E_{sc}(t,\theta,\varphi) d\Omega, \tag{13}$$

where $E_{sc}(t,\theta,\varphi)$ is defined in Equation (7). Consequently, the average power of the spacecraft signal over an integration interval $\mathcal{T}$ is

$$\begin{aligned} P_{sc} =& \langle v_{sc}(t) v_{sc}^*(t) \rangle_{\mathcal{T}} \\ =& S_{sc} A_e \iint\limits_{\Omega_{sc}} \iint\limits_{\Omega_{sc}} \sqrt{F(\theta,\varphi)F(\theta',\varphi')} \langle s(t)s^*(t) \rangle_{\mathcal{T}} \delta(\theta-\theta_0, \varphi-\varphi_0) \delta(\theta'-\theta_0, \varphi'-\varphi_0) d\Omega d\Omega' \\ =& S_{sc} A_e F(\theta_0, \varphi_0) \\ =& \frac{P_t G_t}{L} G(\theta_0, \varphi_0), \end{aligned} \tag{14}$$

where the last equality follows from Assumption (A.9).

B. Thermal Noise

Based on Assumption (A.11), the thermal noise power per polarization is simply equal to

$$P_n = \langle v_n(t) v_n^*(t) \rangle_\tau = kT_n B, \tag{15}$$

where $v_n(t)$ denotes the voltage measured at the output of the antenna due to thermal noise.

C. Interference from the Planetary Body

The voltage at the output of the DSN antenna due to the planetary body and at frequency f is equal to

$$v_p(t) = \frac{\sqrt{A_e}}{\sqrt{2}} \iint\limits_{\Omega_p} \sqrt{F(\theta,\varphi)} E_p(t,\theta,\varphi) d\Omega, \tag{16}$$

where Ω_p is the extent of the planetary body in the sky. The factor $1/\sqrt{2}$ is introduced here because planetary radiation is unpolarized, but, for the purposes of this discussion, the DSN antenna is assumed to receive only one polarization. In turn, the average (polarized) power due to the planet is

$$\begin{aligned} P_p =& \langle \int\limits_B v_p(t) v_p^*(t) df \rangle_\tau \\ =& \frac{A_e}{2} \int\limits_B \iint\limits_{\Omega_p} \iint\limits_{\Omega_p} \sqrt{F(\theta,\varphi) F(\theta',\varphi')} \langle E_p(t,\theta,\varphi), E_p^*(t',\theta',\varphi') \rangle_\tau d\Omega d\Omega' df, \end{aligned} \tag{17}$$

where the integration over the bandwidth of the spacecraft signal B is applied because the spectral brightness of the planet $I_p(f,\theta,\varphi)$ is expressed per unit of frequency.

As stated in Assumption (A.7), the planet radiation is spatially and temporally uncorrelated. Therefore,

$$P_p = \frac{A_e}{2} \int\limits_B \iint\limits_{\Omega_p} F(\theta,\varphi) I_p(f,\theta,\varphi)\, d\Omega df. \tag{18}$$

If we further assume that the planet radiation varies slowly with frequency (see Assumption (A.7)), then we can approximate the value of $I_p(f,\theta,\varphi)$ by that of the spectral brightness at the carrier frequency and assume that it is constant over the spacecraft's signal bandwidth B. This results in

$$P_p \approx \frac{A_e B}{2} \iint\limits_{\Omega_p} F(\theta,\varphi) I_p(f_c,\theta,\varphi) d\Omega, \tag{19}$$

where f_c is the carrier frequency. Next, we substitute the Rayleigh-Jeans approximation for the planet spectral brightness and use the fact that $G_{max} = \frac{4\pi}{\lambda^2} A_e$

to obtain

$$P_p \approx \frac{kB}{4\pi} \iint\limits_{\Omega_p} G(\theta, \varphi) T_b\left(\theta, \varphi\right) d\Omega, \tag{20}$$

an expression that can be further simplified if we consider the planet to have a constant average brightness temperature $\bar{T}_b$ across its solid angle Ω_p. In that case,

$$P_p \approx \frac{k\bar{T}_b B}{4\pi} \iint\limits_{\Omega_p} G(\theta, \varphi) d\Omega. \tag{21}$$

Finally, for a planet of small angular diameter compared to the primary beam of the antenna, and assuming that the planet center is located at coordinates (θ_p, φ_p), we find that

$$P_p \approx \frac{k\bar{T}_b B}{4\pi} G(\theta_p, \varphi_p) \iint\limits_{\Omega_p} d\Omega \approx \frac{k\bar{T}_b B}{4\pi} G(\theta_p, \varphi_p) \pi \psi_p^2, \tag{22}$$

where ψ_p is the angular radius of the planet in radians (as opposed to Ω_p, which is measured in stereo radians). The second equality follows from the solid angle approximation of a spherical cap on the unit sphere [5], which is only valid when ψ_p is small compared to beamwidth of the DSN antenna. Finally, because planetary distances are orders of magnitude larger than the planet diameter, we can use the small-angle approximation so that

$$\tan \psi_p \approx \psi_p = \frac{D_p/2}{L_p}, \tag{23}$$

where D_p is the mean diameter of the planet and L_p is the distance between the planet and Earth at analysis epoch. This results in

$$P_p \approx \frac{k\bar{T}_b B}{16} G(\theta_p, \varphi_p) \left(\frac{D_p}{L_p}\right)^2. \tag{24}$$

In communications systems, it is common practice to characterize sources of noise using their equivalent noise temperature. Let T_p denote the equivalent noise temperature of the planetary body. By definition, the noise power per polarization must be equal to $P_p = kT_pB$. Comparing this expression with Equation (24) yields

$$T_p \approx \frac{\bar{T}_b}{16} G(\theta_p, \varphi_p) \left(\frac{D_p}{L_p}\right)^2, \tag{25}$$

which matches the results reported in Reference [6]. In general, if the angular extent of the planet is not small compared with the antenna beam, then using Equation (21) we get

$$T_p \approx \frac{\bar{T}_b}{4\pi} \iint\limits_{\Omega_p} G(\theta, \varphi) d\Omega. \tag{26}$$

D. SNR and G/T

Using the results in this section, we conclude that the SNR at the output of a DSN antenna (and under a matched load) is

$$\text{SNR} = \frac{P_t G_t}{L} \frac{G(\theta_0, \varphi_0)}{k\,(T_p + T_n)\,B}, \tag{27}$$

where T_p is the equivalent noise temperature of the planet and is given by

$$\begin{aligned} T_p &= \iint_{\Omega_p} G\,(\theta, \varphi)\, T_b\,(\theta, \varphi)\, d\Omega \\ &\approx \frac{\bar{T}_b}{4\pi} \iint_{\Omega_p} G(\theta, \varphi) d\Omega \\ &\approx \frac{k \bar{T}_b B}{16} G(\theta_p, \varphi_p) \left(\frac{D_p}{L_p} \right)^2, \end{aligned} \tag{28}$$

with the approximations valid under the conditions defined in the previous section. Finally, the equivalent G/T of the DSN antenna is defined as

$$\frac{G}{T} = \frac{G(\theta_0, \varphi_0)}{T_p + T_n}. \tag{29}$$

III. Analysis for an Array of Antennas

We now consider the case of N DSN antennas operating in downlink array mode.[3] All antennas are pointed toward the spacecraft, which, per Assumption (A.10), is located at (θ_0, φ_0). Additionally, they all receive planetary noise from a nearby body, located in an angular extent Ω_p. Note that while (θ_0, φ_0) may be contained in Ω_p, in general this need not be the case.

A. Spacecraft Signal

Let $\tau_i\,(\theta, \varphi)$ denote the excess delay experienced by an EM front-wave arriving from direction (θ, φ), measured from the center of the array, which we define arbitrarily (thus τ_i can be positive or negative). Then, the voltage measured at the output of the i-th DSN antenna from the spacecraft transmission is

$$v^i_{sc}(t) = \sqrt{A_e} \iint_{\Omega_{sc}} \sqrt{F_i(\theta, \varphi)} E^i_{sc}(t, \theta, \varphi) e^{-j 2\pi f_c \tau_i(\theta, \varphi)} d\Omega, \tag{30}$$

[3] To facilitate the discussion, we will assume that all antennas are homogeneous. Extensions to the case of a heterogeneous array, such as a combination of DSN 34-m BWG antennas and DSN 70-m antennas, is straightforward.

where the term $e^{-j2\pi f_c \tau_i(\theta,\varphi)}$ is the phase shift inherent to the i-th array element due to its position relative to the array center;[4]

$$E^i_{sc}(t,\theta,\varphi) = \sqrt{S_{sc}} s(t-\tau_i(\theta,\varphi)) e^{-j\phi_i(\theta,\varphi)} \delta(\theta-\theta_0, \varphi-\varphi_0) \tag{31}$$

is the far-field complex electric field radiated by the spacecraft, in volts per meter; and $\phi_i(\theta_0,\varphi_0)$ is an unknown phase that models additional phase terms from factors such as the atmosphere or the fact that the DSN performs full-spectrum combining using intermediate frequency (IF) signals [7]. Therefore,

$$\begin{aligned} v^i_{sc}(t) =& \sqrt{S_{sc}A_e} \iint_{\Omega_{sc}} \sqrt{F_i(\theta,\varphi)} s(t-\tau_i(\theta,\varphi)) e^{-j\xi_i(\theta,\varphi)} \delta(\theta-\theta_0,\varphi-\varphi_0) d\Omega \\ =& \sqrt{S_{sc}A_e F_i(\theta_0,\varphi_0)} s(t-\tau_i(\theta_0,\varphi_0)) e^{-j\xi_i(\theta_0,\varphi_0)} \\ =& \sqrt{\tfrac{P_t G_t}{L} G_i(\theta_0,\varphi_0)} s(t-\tau_i(\theta_0,\varphi_0)) e^{-j\xi_i(\theta_0,\varphi_0)}, \end{aligned} \tag{32}$$

where

$$\xi_i(\theta_0,\varphi_0) = \phi_i(\theta_0,\varphi_0) + 2\pi f_c \tau_i(\theta_0,\varphi_0) \tag{33}$$

is the total phase misalignment for the i-th antenna and $\tau_i(\theta_0,\varphi_0)$ is the time misalignment.

In arrayed operations, the output voltage of the array is calculated by coherently summing a scaled, delayed, and phase-shifted version of the signals received via each array element. In other words, in general we may write the voltage at the output of the array correlator as

$$v_{sc}(t) = \sum_{\forall i} a_i e^{j\psi_i} v^i_{sc}(t+\mu_i), \tag{34}$$

where $a_i \in \mathbb{R}$ is a scaling constant, and ψ_i and μ_i compensate the phase and time misalignment, respectively. Thus,

$$\begin{aligned} v_{sc}(t) =& \sqrt{\tfrac{P_t G_t}{L}} \sum_{\forall i} \sqrt{G_i(\theta_0,\varphi_0)} s(t-\tau_i(\theta_0,\varphi_0)+\mu_i) a_i(\theta_0,\varphi_0) e^{j\psi_i} e^{-j\xi_i(\theta_0,\varphi_0)} \\ =& \sqrt{\tfrac{P_t G_t}{L}} \sum_{\forall i} \sqrt{G_i(\theta_0,\varphi_0)} s(t-\tau_i(\theta_0,\varphi_0)+\mu_i) w_i(\theta_0,\varphi_0) e^{-j2\pi f_c \tau_i(\theta_0,\varphi_0)} \end{aligned} \tag{35}$$

where

$$w_i(\theta_0,\varphi_0) = a_i e^{j[\psi_i - \phi_i(\theta_0,\varphi_0)]} \tag{36}$$

is a complex phasor that weighs the voltage received via each antenna. Next, assume that all antennas have similar radiation patterns and that the array correlator is able

[4] Some references use an alternative but equivalent notation such that this term is expressed as e^{-jkr_i}, where $k = \frac{2\pi}{\lambda}$ is the wave number and r_i is the distance from the array element position to the array center.

to estimate the time delay for each element in the array accurately, i.e., $\mu_i = \hat{\tau}_i(\theta_0, \varphi_0) \approx \tau_i(\theta_0, \varphi_0)$. Then,

$$\begin{aligned} v_{sc}(t) \approx & \sqrt{\tfrac{P_t G_t}{L} G(\theta_0, \varphi_0)} s(t) \sum_{\forall i} w_i(\theta_0, \varphi_0) e^{-j2\pi f_c \tau_i(\theta_0, \varphi_0)} \\ = & \sqrt{\tfrac{P_t G_t}{L} G(\theta_0, \varphi_0)} s(t) AF(\theta_0, \varphi_0), \end{aligned} \tag{37}$$

where

$$AF(\theta, \varphi) = \sum_{\forall i} w_i(\theta_0, \varphi_0) e^{-j2\pi f_c \tau_i(\theta, \varphi)} \tag{38}$$

is known in the literature as the array factor. Similarly, the power at the output of the array becomes

$$\begin{aligned} P_{sc} = & \langle v_{sc}(t) v_{sc}^*(t) \rangle_{\mathcal{T}} \\ = & \tfrac{P_t G_t}{L} \langle |s(t)|^2 \rangle_{\mathcal{T}} \sum_{\forall i} \sum_{\forall j} w_i w_j^* \sqrt{G_i(\theta_0, \varphi_0) G_j(\theta_0, \varphi_0)} e^{-j2\pi f_c \tau_{ij}(\theta_0, \varphi_0)} \\ = & \tfrac{P_t G_t}{L} G(\theta_0, \varphi_0) \sum_{\forall i} \sum_{\forall j} w_i w_j^* e^{-j2\pi f_c \tau_{ij}(\theta_0, \varphi_0)} \\ = & \tfrac{P_t G_t}{L} G(\theta_0, \varphi_0) |AF(\theta_0, \varphi_0)|^2, \end{aligned} \tag{39}$$

where the third equality is true because I have assumed identical array elements and $\tau_{ij}(\theta, \varphi)$ is defined as

$$\tau_{ij}(\theta, \varphi) = \tau_i(\theta, \varphi) - \tau_j(\theta, \varphi). \tag{40}$$

Thus, if we define the gain of the array as $G_{arr}(\theta, \varphi) = G(\theta, \varphi) |AF(\theta, \varphi)|^2$, then

$$P_{sc} = \tfrac{P_t G_t}{L} G_{arr}(\theta_0, \varphi_0). \tag{41}$$

Key to the array operation is to select values of a_i, ψ_i, and μ_i such that the array experiences maximal gain in the direction of the spacecraft. In the case of the DSN, the correlator at each complex achieves this by performing the following steps:

- The time and phase misalignments of the signal from each antenna are estimated. In other words, values for $\hat{\tau}_i(\theta_0, \varphi_0)$ and $\hat{\xi}_i(\theta_0, \varphi_0)$ are constantly generated during an array track.[5]
- The signal received by each antenna is first time-aligned by setting $\mu_i = \hat{\tau}_i(\theta_0, \varphi_0)$ and delaying the signals from each antenna by the corresponding amount.[6]

[5] In the actual DSN implementation, delay and Doppler post-compensation are applied. For the purposes of the discussion, we may assume that those are incorporated into the estimates $\hat{\tau}_i(\theta_0, \varphi_0)$ and $\hat{\xi}_i(\theta_0, \varphi_0)$ generated by the correlator.

[6] Technically, a backwards time shift of μ_i seconds cannot be implemented. This is simply fixed by delaying all signals by $\mu_i = \Delta + \hat{\tau}_i(\theta_0, \varphi_0)$ with Δ large enough so that all time shifts are positive.

- The time-aligned signal is then multiplied by a normalized complex phasor $e^{j\psi_i}$, $\psi_i = \hat{\xi}_i(\theta_0, \varphi_0)$. This phasor phase-aligns the signal received by each element of the array from the spacecraft direction (θ_0, φ_0). In other words, it effectively steers the main beam of the array toward the spacecraft.
- The time- and phase-aligned signals from each antenna are weighted by a real value a_i, which is calculated to maximize the SNR at the output of the array. Under the assumption of a homogeneous array (same gain, same equivalent noise temperature), these coefficients are all equal, so they can be normalized to unity [2].[7]
- The weighted, time- and phase-aligned signals are summed coherently, in voltage.

Based on this process, we see that

$$\begin{aligned} AF(\theta_0, \varphi_0) &= \sum_{\forall i} w_i(\theta_0, \varphi_0) e^{-j2\pi f_c \tau_i(\theta_0, \varphi_0)} \\ &= \sum_{\forall i} e^{j[\psi_i - \phi_i(\theta_0, \varphi_0)]} e^{-j2\pi f_c \tau_i(\theta_0, \varphi_0)} \\ &= \sum_{\forall i} e^{j\psi_i} e^{-j[\phi_i(\theta_0, \varphi_0) + 2\pi f_c \tau_i(\theta_0, \varphi_0)]} \\ &= \sum_{\forall i} e^{j\left[\hat{\xi}_i(\theta_0, \varphi_0) - \xi_i(\theta_0, \varphi_0)\right]} \\ &\approx \sum_{\forall i} 1 = N, \end{aligned} \tag{42}$$

where the fourth equality follows from assuming that the correlator produces phase estimates $\psi_i = \hat{\xi}_i(\theta_0, \varphi_0) \approx \xi_i(\theta_0, \varphi_0)$. Similarly,

$$G_{arr}(\theta_0, \varphi_0) = |AF(\theta_0, \varphi_0)|^2 G(\theta_0, \varphi_0) = N^2 G(\theta_0, \varphi_0). \tag{43}$$

Combining these results we conclude that for homogeneous array elements

$$v_{sc}(t) \approx \sqrt{\frac{P_t G_t}{L} G(\theta_0, \varphi_0)} N s(t) \tag{44}$$

and

$$P_{sc} \approx \frac{P_t G_t}{L} G(\theta_0, \varphi_0) N^2. \tag{45}$$

Note that the array factor is only equal to N in the direction of the spacecraft (θ_0, φ_0) where the array has been phased up.

B. Thermal Noise

Each antenna in the array experiences uncorrelated thermal noise per Assumption (A.11). Therefore, the total noise power per polarization at the output of the array

[7] See Reference [2], Appendix D for a derivation of these coefficients.

processor is

$$P_n = \sum_{\forall i} P_n^i = \sum_{\forall i} kT_n^i B = k\left[\sum_{\forall i} T_n^i\right] B. \tag{46}$$

This indicates that the total noise temperature of the array is the sum of the individual noise temperatures "seen" by each antenna. If all elements in the array are homogeneous and they all operate under similar thermal noise conditions, this results in

$$P_n = k(NT_n)B. \tag{47}$$

Consequently, if we ignore the contribution of the planetary body, the G/T of the array becomes

$$\frac{G}{T}_{arr} = \frac{N^2 G(\theta,\varphi)}{NT_n} = N\frac{G}{T}_{1} \tag{48}$$

with $\frac{G}{T}_{1}$ equal to the G/T of one element in the array. This is the well-known theoretical gain of an array of DSN antennas operating in the downlink direction.

C. Interference from the Planetary Body

The voltage measured at the output of the i-th DSN antenna in the array because of the planet contribution can be expressed as

$$v_p^i(t) = \frac{\sqrt{A_e}}{\sqrt{2}} \iint\limits_{\Omega_p} \sqrt{F(\theta,\varphi)} E_p(t,\theta,\varphi) e^{-j\phi_i(\theta,\varphi)} e^{-j2\pi f \tau_i(\theta,\varphi)} d\Omega. \tag{49}$$

Note that in this expression the phase shift experienced by the planetary radiation depends both on frequency f (as opposed to f_c, which is a constant) and direction of arrival (θ,φ). At the output of the array processor, the voltage from all antennas is summed coherently according to[8]

$$\begin{aligned} v_p(t) =& \sum_{\forall i} a_i e^{j\psi_i} v_p^i(t) \\ =& \frac{\sqrt{A_e}}{\sqrt{2}} \iint\limits_{\Omega_p} \sqrt{F(\theta,\varphi)} E_p(t,\theta,\varphi) \sum_{\forall i} a_i e^{j[\psi_i - \phi_i(\theta,\varphi)]} e^{-j2\pi f \tau_i(\theta,\varphi)} \\ =& \frac{\sqrt{A_e}}{\sqrt{2}} \iint\limits_{\Omega_p} \sqrt{F(\theta,\varphi)} E_p(t,\theta,\varphi) \sum_{\forall i} w_i(\theta,\varphi) e^{-j2\pi f \tau_i(\theta,\varphi)} \\ =& \frac{\sqrt{A_e}}{\sqrt{2}} \iint\limits_{\Omega_p} \sqrt{F(\theta,\varphi)} E_p(t,\theta,\varphi) A F_p(f,\theta,\varphi). \end{aligned} \tag{50}$$

[8] Because the planet is a source of uncorrelated noise, the effect of the time shift due to μ_i is irrelevant. Therefore, it is obviated in this section to ease notation.

with

$$AF_p(f,\theta,\varphi) = \sum_{\forall i} w_i(\theta,\varphi) e^{-j2\pi f \tau_i(\theta,\varphi)}. \tag{51}$$

$AF_p(f,\theta,\varphi)$ can be interpreted as the equivalent array factor experienced by the planetary body, which depends on both frequency and the angle of arrival of the planetary radiation.

The power contribution from the planetary body at the output of the array processor is

$$\begin{aligned}
P_p =& \langle \int_B v_p(t) v_p^*(t) df \rangle_\tau \\
=& \frac{A_e}{2} \int_B \iint_{\Omega_p} \iint_{\Omega_p} \sqrt{F_i(\theta,\varphi) F_j(\theta',\varphi')} \Xi_p^i AF_p(f,\theta,\varphi) AF_p^*(f,\theta',\varphi') d\Omega d\Omega' df \\
=& \frac{A_e}{2} \iint_{\Omega_p} F(\theta,\varphi) \int_B I_p(f,\theta,\varphi) |AF_p(f,\theta,\varphi)|^2 df d\Omega \\
\approx& \frac{A_e}{2} \iint_{\Omega_p} F(\theta,\varphi) I_p(f_c,\theta,\varphi) \int_B |AF_p(f,\theta,\varphi)|^2 df d\Omega,
\end{aligned} \tag{52}$$

where $\Xi_p^i = \langle E_p^i(t,\theta,\varphi) E_p^{i*}(t',\theta',\varphi') \rangle_\tau$ is calculated using Assumption (A.7) and the narrowband approximation is used once again. Next, we expand the term containing the array factor by noting that

$$\begin{aligned}
\int_B |AF_p(f,\theta,\varphi)|^2 df =& \sum_{\forall i} \sum_{\forall j} w_i(\theta,\varphi) w_j^*(\theta,\varphi) \int_B e^{-j2\pi f \tau_{ij}(\theta,\varphi)} df \\
=& \sum_{\forall i} \sum_{\forall j} w_i(\theta,\varphi) w_j^*(\theta,\varphi) \Lambda_{ij}(\theta,\varphi)
\end{aligned} \tag{53}$$

with

$$\begin{aligned}
\Lambda_{ij}(\theta,\varphi) =& \int_{f_c - B/2}^{f_c + B/2} e^{-j2\pi f \tau_{ij}(\theta,\varphi)} df \\
=& \int_{-B/2}^{+B/2} e^{-j2\pi (u+f_c) \tau_{ij}(\theta,\varphi)} du \\
=& e^{-j2\pi f_c \tau_{ij}(\theta,\varphi)} \int_{-B/2}^{+B/2} e^{-i2\pi u \tau_{ij}(\theta,\varphi)} du \\
=& e^{-j2\pi f_c \tau_{ij}(\theta,\varphi)} B \mathrm{sinc}\left(B\tau_{ij}\left(\theta,\varphi\right)\right)
\end{aligned} \tag{54}$$

where $\mathrm{sinc}\left(x\right) = \frac{\sin(\pi x)}{x}$ and the antenna filter has been assumed to be rectangular with bandwidth B, equal to the spacecraft's signal bandwidth. Define

$$\tilde{\Lambda}_{ij}(\theta,\varphi) = \frac{\Lambda_{ij}(\theta,\varphi)}{B} = e^{-j2\pi f_c \tau_{ij}(\theta,\varphi)} \mathrm{sinc}\left(B\tau_{ij}(\theta,\varphi)\right) \tag{55}$$

as the bandwidth-normalized delay beam and apply the Rayleigh-Jeans approximation. Then,

$$P_p = \frac{kB}{4\pi} \iint\limits_{\Omega_p} T_{bb}(\theta,\varphi)\sqrt{G_i(\theta,\varphi)G_j(\theta,\varphi)}|AF_p(\theta,\varphi)|^2 d\Omega, \tag{56}$$

where, in an abuse of notation, we have defined

$$|AF_p(\theta,\varphi)|^2 = \sum_{\forall i}\sum_{\forall j} w_i(\theta,\varphi)w_j^*(\theta,\varphi)\tilde{\Lambda}_{ij}(\theta,\varphi), \tag{57}$$

which is slightly different from $|AF_p(f,\theta,\varphi)|^2$ as defined by Equation (53). Further straightforward simplifications are now possible for arrays of homogeneous antennas and for planets with approximately constant average brightness temperature. In particular:

$$P_p = \frac{k\bar{T}_b B}{4\pi} \iint\limits_{\Omega_p} G(\theta,\varphi)|AF_p(\theta,\varphi)|^2 d\Omega \tag{58}$$

and

$$T_p = \frac{\bar{T}_b}{4\pi} \iint\limits_{\Omega_p} G(\theta,\varphi)|AF_p(\theta,\varphi)|^2 d\Omega. \tag{59}$$

1. Narrowband Operation

We have shown that the equivalent array factor for the planetary body is

$$|AF_p(\theta,\varphi)|^2 = \sum_{\forall i}\sum_{\forall j} w_i(\theta,\varphi)w_j^*(\theta,\varphi)\tilde{\Lambda}_{ij}(\theta,\varphi) \tag{60}$$

where

$$\tilde{\Lambda}_{ij}(\theta,\varphi) = e^{-j2\pi f_c \tau_{ij}(\theta,\varphi)}\text{sinc}\left(B\tau_{ij}(\theta,\varphi)\right). \tag{61}$$

Furthermore, we know from Equation (3) that

$$\tau_{ij}(\theta,\varphi) = \tau_i(\theta,\varphi) - \tau_j(\theta,\varphi) = \frac{\vec{\mathbf{B}}_{ji}\cdot\hat{\mathbf{r}}_0(\theta,\varphi)}{c} = \frac{B_{ji}}{c}\hat{\mathbf{B}}_{ji}\cdot\hat{\mathbf{r}}_0(\theta,\varphi), \tag{62}$$

where $\vec{\mathbf{B}}_{ji} = \vec{\mathbf{r}}_j - \vec{\mathbf{r}}_i$ is the baseline between the i-th and j-th antenna. Hence,

$$|\tau_{ij}(\theta,\varphi)| \leq \frac{B_{ij}}{c} \leq \frac{D_{arr}}{c}, \tag{63}$$

where D_{arr} is the array diameter, defined as the maximum across all baselines.

Assume the spacecraft transmits a signal with bandwidth B such that $B\frac{D_{arr}}{c} \approx 0$. Then, using Equation (63) we find that

$$\text{sinc}\left(B\tau_{ij}(\theta,\varphi)\right) \approx 1 \;\forall(i,j) \tag{64}$$

so that

$$\tilde{\Lambda}_{ij}(\theta,\varphi) \approx e^{-j2\pi f_c \tau_{ij}(\theta,\varphi)} \tag{65}$$

and

$$|AF_p(\theta,\varphi)|^2 \approx \sum_{\forall i}\sum_{\forall j} w_i(\theta,\varphi) w_j^*(\theta,\varphi) e^{-j2\pi f_c \tau_{ij}(\theta,\varphi)}. \tag{66}$$

Additionally, we may assume that the phase ϕ_i experienced by the planet's radiation from a differential of area at coordinates (θ,φ) is approximately equal to that experienced by the spacecraft signal.[9] In other words, $\phi(\theta,\varphi) \approx \phi(\theta_0,\varphi_0)\,\forall(\theta,\varphi) \in \Omega_p$ so that

$$|AF_p(\theta,\varphi)|^2 \approx \sum_{\forall i}\sum_{\forall j} w_i(\theta_0,\varphi_0) w_j^*(\theta_0,\varphi_0) e^{-j2\pi f_c \tau_{ij}(\theta,\varphi)} = |AF(\theta,\varphi)|^2. \tag{67}$$

Thus, we conclude that for an array of homogeneous antennas viewing a planetary body with approximately constant brightness temperature in a narrow band,

$$P_p \approx \frac{k\bar{T}_b B}{4\pi} \iint\limits_{\Omega_p} G_{arr}(\theta,\varphi) d\Omega, \tag{68}$$

where $G_{arr}(\theta,\varphi) = G(\theta,\varphi)\,|AF(\theta,\varphi)|^2$. Similarly, the effective noise temperature of the planet is

$$T_p \approx \frac{\bar{T}_b}{4\pi} \iint\limits_{\Omega_p} G_{arr}(\theta,\varphi) d\Omega. \tag{69}$$

For a planet of small angular diameter compared to the main beam of the array, we can use the same reasoning as in Equations (22)–(25) and approximate the noise temperature by

$$T_p \approx \frac{\bar{T}_b}{16} G_{arr}(\theta_p,\varphi_p) \left(\frac{D_p}{L_p}\right)^2 \tag{70}$$

which, for an array of homogeneous antennas, is upper bounded by

$$T_p \lesssim \frac{\bar{T}_b}{16} N^2 G(\theta_p,\varphi_p) \left(\frac{D_p}{L_p}\right)^2 = N^2 \tilde{T}_p, \tag{71}$$

where $\tilde{T}_p$ is the noise temperature "seen" when tracking the spacecraft with a single antenna (see Equation (25)).

D. Array SNR and G/T

The SNR of an array of DSN antennas receiving a narrowband signal from a spacecraft close to a planetary body can be estimated as

$$\text{SNR} = \frac{P_{sc}}{P_p + P_n} = \frac{P_t G_t}{L} \frac{G_{arr}(\theta_0,\varphi_0)}{k\,(T_p + T_n)\,B} \tag{72}$$

---

[9] This is a reasonable assumptions because (1) the spacecraft is close to the hot body, so its radiation goes through the same atmosphere as the spacecraft signal, approximately; and (2) the downconversion process applies equally to the spacecraft signal and the hot body radiation.

where T_p is calculated as in Equation (69). For non-narrowband operation, T_p must be adjusted to properly account for the beam delay using Equation (59). Similarly, the G/T of the system can be calculated as

$$\frac{G}{T}_{arr} = \frac{G_{arr}(\theta_0, \varphi_0)}{T_p + T_n}. \tag{73}$$

E. Numerical Example for an Array of 34-m BWG Antennas

We now provide a short numerical example to exemplify some of the equations derived in this section. For simplicity, we assume narrowband operation so that the array performance is characterized by $G_{arr}(\theta, \varphi)$.

Consider the array of Figure 2 with three DSN 34-m BWG antennas (DSS-34, DSS-35, and DSS-36) tracking the Juno spacecraft at X-band. Using trajectory information from the DSN, we calculate the position of all elements at epoch 2023-03-01 2:31:00 UTC and estimate the gain of a single 34-m BWG antenna, the array factor, and the gain of the resulting array. For the latter, phasing of the array is assumed ideal, and all phases are calculated using DSS-35 as the designated array origin.

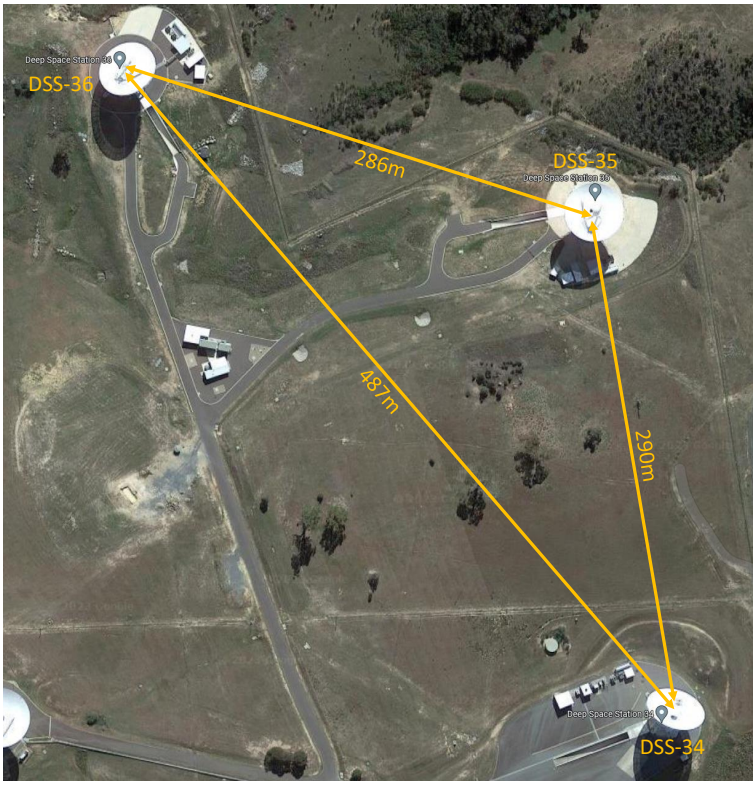

Figure 2. Satellite map of DSS-34, DSS-35 and DSS-36 in the Canberra Deep Space Communications Complex. The array diameter is ~ 500 m, corresponding to array angular resolution of ~ 0.07 mrad.

Figure 3 plots the results of this analysis with azimuth and elevation expressed relative

to the position of the spacecraft. It can be observed that the array factor contains several "gain peaks" within the primary beam of a DSN 34-m BWG antenna, which is centered at (0,0). The value of these peaks is close to the maximum gain of the array (equal to 77.6 dB, 68.1 dB from a single antenna, plus 9.5 dB from the array factor); thus, hot body noise radiation arriving from these directions will contribute significantly to the array performance.

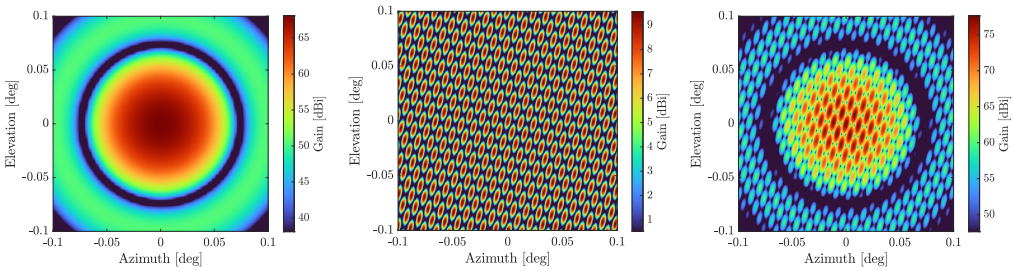

(a) Gain of one DSN 34-m BWG antenna **(b) Array factor of the 3-element array** **(c) Gain of the 3-element array**

Figure 3. Gain of the 3-element array in Figure 2 when tracking Juno at epoch 2023-03-01 2:31:00 UTC. Color scales for each plot are different.

As a second example, Figure 4 plots the gain of the array under the same configuration when only two DSN 34-m BWG antennas are used (DSS-34 and DSS-35). In this case, the grating lobes are wider, suggesting that the 2-element array will not only have less gain compared to a 3-element array but also suffer from additional hot body noise contribution when tracking a spacecraft close to a planetary body.

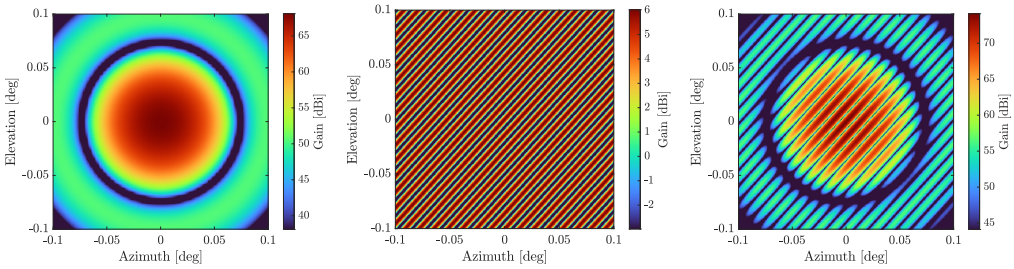

(a) Gain of one DSN 34-m BWG antenna **(b) Array factor of the 2-element array** **(c) Gain of the 2-element array**

Figure 4. Gain of the 2-element array formed by DSS-34 and DSS-35 when tracking Juno at epoch 2023-03-01 2:31:00 UTC. Color scales for each plot are different.

A key characteristic of an array of DSN antennas is that all elements are separated by distances orders of magnitude larger than $\lambda_c/2$. Consequently, the array factor has high directivity, but it also exhibits a large number of grating lobes (also known as fringes in the literature), which are defined as main beam lobes in directions other than the array boresight direction [3]. These grating lobes can be clearly observed in Figures 3b and 3c, and they cause peaks of directivity centered in directions other than (0,0). Their effect on hot body noise is further analyzed in the following sections.

IV. Classification of Noise Sources

We now consider how a source of hot body noise contributes to system performance as a function of the array configuration and the source's angular extent Ω_p. In particular, we consider two cases:

1. Extended source: Ω_p is large compared to the main beam of the array. Noise may be "picked up" via the main beam, and/or via one or multiple grating lobes, which act as sources of correlated noise.
2. Compact source: Ω_p is small compared to the main beam of the array. Noise may be picked up via the main beam or via one of the grating lobes, depending on the relative position of the planet and the spacecraft.

To formalize these cases, let us define a metric ξ that measures the ratio of planetary angular radius ψ_p to angular extent of the array main beam ψ_{arr}:

$$\xi = \frac{\psi_p}{\psi_{arr}}. \tag{74}$$

From Equation (23) we know that

$$\psi_p \propto \frac{R_p}{L_p}, \tag{75}$$

where R_p is the planet radius and L_p is the distance to Earth at the epoch of analysis. Similarly, it is known that the angular extent of the main beam of the array is proportional to

$$\psi_{arr} \propto \frac{\lambda_c}{D_{arr}}, \tag{76}$$

where λ_c is the carrier wavelength and D_{arr} is the array diameter defined in Section III.C.1 [3].[10] Therefore,

$$\xi \propto \frac{D_{arr}}{\lambda_c}\frac{R_p}{L_p}, \tag{77}$$

and a source can be categorized as extended when $\xi \gtrsim 1$ or compact when $\xi \ll 1$. This result indicates that a body like Mars, for which L_p varies significantly over a synodic period, may be both an extended or compact source depending on the time of the year. Similarly, a source may be classified as extended or compact depending on the specific DSN antennas used in the array, which varies its diameter. Hence, from Equation (77) we conclude that a source is not inherently extended or compact; it can be made extended or compact by changing the properties of the array.

Figure 5 plots the value of ξ vs. distance to Earth for the main bodies of the solar system and as a function of the frequency band of operation. The color of the marker

[10] Equation (76) approximately defines the maximum angular resolution of the array beam as determined by the orientation of the largest separation between array elements.

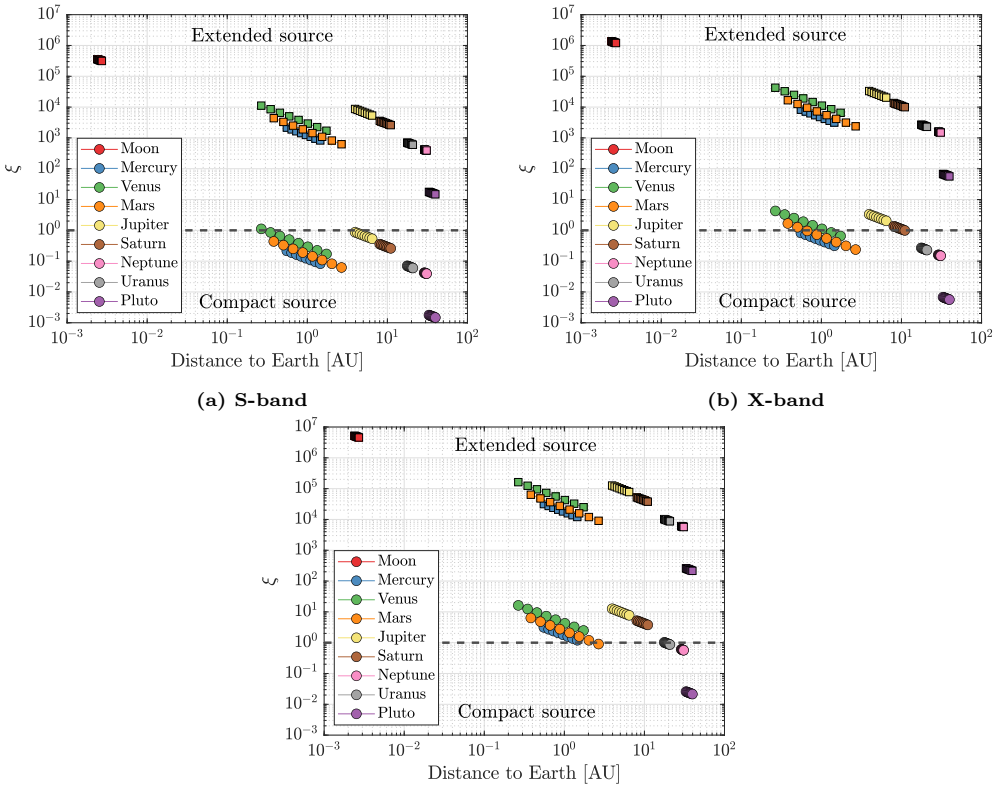

Figure 5. Categorization of solar system bodies as extended or point sources. Circles and squares indicate cases where intra-site and inter-site arraying is assumed, respectively. The dashed black line indicates the transition region from a compact to an extended source.

indicates the body being considered, while the type of marker (circle vs. asterisk) indicates the assumed array diameter. For intra-complex arraying (circles), it is assumed that the array diameter is 1 km (see Appendix I), while inter-complex arraying (asterisks) assumes 10,000 km. We observe that for intra-complex arraying, which is currently performed by the DSN, only Neptune, Uranus, and Pluto can be considered point sources. However, if the DSN performed inter-complex arraying, then all bodies would be extended sources.

A. Extended Sources

We now consider the case of an extended source. The amount of hot body noise received by the antenna depends on the position of the planetary body relative to the position of the main beam of the array *and* the grating lobes, which vary over time as the array tracks the spacecraft. For example, Figure 6 shows the angular extent of Jupiter when tracked by an array of three DSN 34-m BWG antennas operating at Ka-band and assuming that the spacecraft is right in front of the planet, as seen from Earth (see block dot). In this case, contributions of hot body noise will come from the main lobe centered around (0,0), as well as the six grating lobes around it.

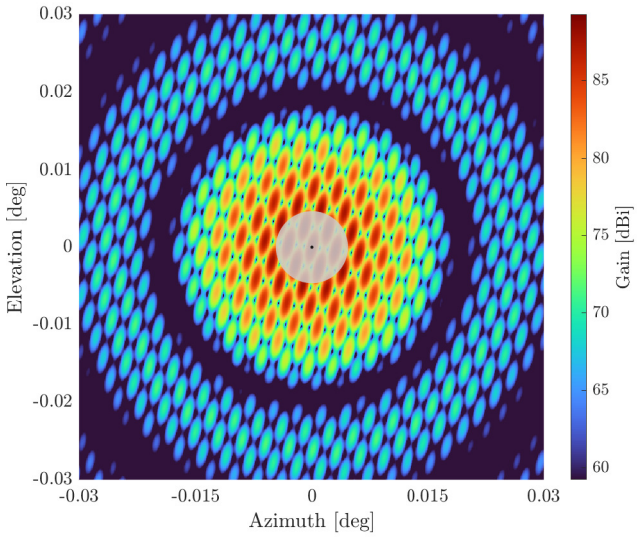

Figure 6. Gain of a 3-element array operating at Ka-band compared to the angular size of Jupiter (gray circle) when the planet is at 5.7 astronomical units from Earth.

Because the location and shape of the grating lobes varies over time with the spacecraft trajectory and the relative orientation of the array elements with respect to the spacecraft, accurate estimation of the hot body noise contribution can only be accomplished numerically, by simulating the time-evolution of the array gain while propagating the spacecraft trajectory. An example of this approach is provided in Section V for the case of a Juno flyby.

That said, it is interesting to consider the limiting case for the array gain that is achievable for extremely extended sources (which, as noted earlier, may be caused by selecting an arraying with extremely long baselines). To that end, let us define β as the ratio of G/T between the array and a single antenna. For the case of an extended source, this metric is equal to

$$\beta_{\text{extended}} = \frac{\frac{N^2 G(\theta_0,\varphi_0)}{NT_n+T'_p}}{\frac{G(\theta_0,\varphi_0)}{T_n+T_p}} = N^2 \frac{T_n+T_p}{NT_n+T'_p}, \tag{78}$$

where N and T_n are defined as before, T'_p is hot body noise temperature as seen by the array, and T_p is the same quantity as seen by a single element of the array. For a hot body with given angular extent, this source can be made increasingly extended by further separating the array elements, which effectively reduces ψ_{arr}. This causes the main beam of the array to be more directive but also reduces the angular separation of the grating lobes (and increases their directivity). Thus, the density of grating lobes that fit within the planetary disk grows, ultimately filling it entirely and resulting in a total received noise that is approximately N^2 times larger than the amount that would be received by a single antenna. Mathematically, in the limit we expect $T'_p \to N^2 T_p$,

which results in

$$\beta_{\text{extended}} \approx N \frac{1 + \frac{T_n}{T_p}}{N + \frac{T_n}{T_p}}. \tag{79}$$

In the limit, as N grows, the system performance tends to $\beta \approx 1 + \frac{T_n}{T_p}$ because the entire extended source is "seen" as generating correlated noise. Note, however, that this effect can be mitigated by randomizing the position of the array elements in such a way that grating lobes are severely attenuated. In that case, T_p' will be significantly smaller than $N^2 T_p$ and the array performance will continue to improve as N grows.

B. Compact Sources

We consider the case of a compact source and assume it can be well approximated as a point source (i.e., $\xi \ll 1$). In this case, the noise contribution will depend primarily on whether the point source is located within the main beam of the array or within one of the adjacent grating lobes. In either case, the net gain experienced by the hot body noise radiation arriving from the compact source will be approximately ηN, where η is a reduction factor caused by the radiation pattern of each element in the array. For grating lobes very close to the main beam, we may assume $\eta \approx 1$ so that

$$\frac{G}{T}_{arr} \approx \frac{NG(\theta_0, \varphi_0)}{T_n + NT_p} = \frac{G(\theta_0, \varphi_0)}{\frac{T_n}{N} + T_p}, \tag{80}$$

where T_p is equal to the hot body noise temperature "seen" by one antenna in the array. Therefore, we see that the effect of independent thermal noise at each element of the array is progressively reduced as N increases, but the hot body acts as a single source of perfectly correlated noise that drives the system performance. In fact,

$$\lim_{N \to \infty} \frac{G}{T}_{arr} = \frac{G(\theta_0, \varphi_0)}{T_p}, \tag{81}$$

which sets an upper bound on the array G/T. This contrasts with extended sources, for which array performance can always be improved by adding more elements (as long as these new elements do not increase the array diameter and change the type of source, and their positions are properly randomized to minimize grating lobes).

Finally, we consider the improvement in G/T for an array with a compact source. In this case, we obtain that in the limit of a point source

$$\beta_{\text{compact}} \approx \frac{\frac{NG(\theta_0, \varphi_0)}{T_n + NT_p}}{\frac{G(\theta_0, \varphi_0)}{T_n + T_p}} = N \frac{1 + \frac{T_n}{T_p}}{N + \frac{T_n}{T_p}}, \tag{82}$$

which is the same result we obtained for an very extended source. This is because, once again, the entire hot body is "seen" as a single source of correlated noise, albeit in this case it is a point source located exactly at the peak of the array's radiation pattern. Also, similar very extended sources, β_{compact} is upper bounded by $1 + \frac{T_n}{T_p}$ as N grows, but in this case this limiting value will be valid regardless of the relative

position of the array elements. Thus, for cases in which the thermal noise is small compared to the hot body noise (as may be the case for the DSN), the improvement factor of the array when tracking a spacecraft close of a bright point source (i.e., $T_p \gg T_n$) will simply be equal to 1 (i.e., no improvement).

V. Juno Flyby

This section provides a numerical example that demonstrates how the equations in this article can be used to estimate the performance of an array of 34-m BWG antennas when operating close to the a source of hot body noise. In particular, we consider Juno as a test case and analyze the flyby executed by the mission at the beginning of March 2023. Figure 7 plots the elevation of Juno as seen from DSS-35 as a function of time. It also shows the path in the sky traced by Juno as it was flying by Jupiter.

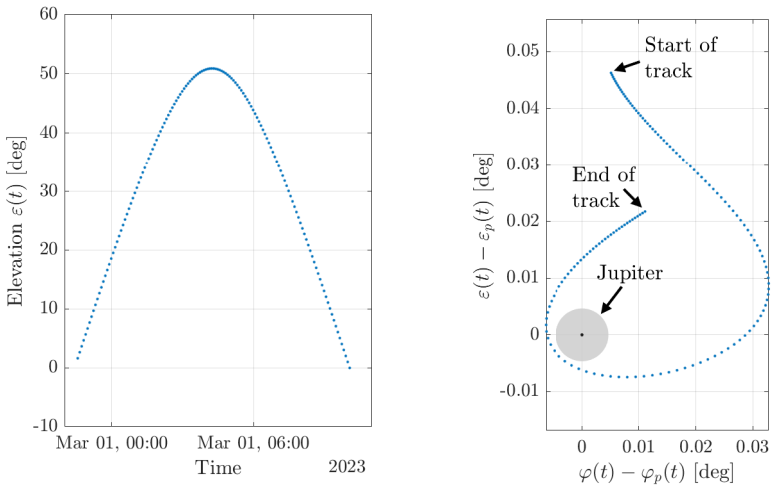

Figure 7. Juno trajectory as it flies by Jupiter in 5-second intervals.

Using this information we now compute the effect of Jupiter as a hot body source. From Reference [6] we assume that the planet's average brightness temperature is 152 K and compare the performance of an array of three 34-m BWG antennas (DSS-34, DSS-35, and DSS-36), a single 34-m BWG antenna (DSS-35), and a DSN 70-m antenna (DSS-43). We perform the calculations assuming operation at both X-band and Ka-band, even though the DSN 70-m antenna currently does not support Ka-band. Additionally, we assume that all antennas experience the same thermal noise, 35 K at X-band and 80 K at Ka-band, and that the aperture efficiency is 75% at X-band and 71% at Ka-band for the 34-m BWG antenna and 50% for the 70-m antenna. Note that these are reasonable numbers given current DSN capabilities, but better estimates could be obtained following the equations in Reference [8].

Estimation of the effective noise temperature for all cases is performed numerically by propagating the spacecraft trajectory and integrating the gain of the antennas and

array over Jupiter's blackbody disk. To ensure numerical stability and reduce computational burden, integration is only performed over an angular extent equal to 5.5 times the half-power beamwidth of one 34-m BWG antenna. This is sufficient to capture the main beam of the antenna as well as the secondary lobe, which is attenuated by at least 17 dB. Thus hot body noise contributions from parts of the radiation pattern that are omitted can be safely assumed to be negligible.

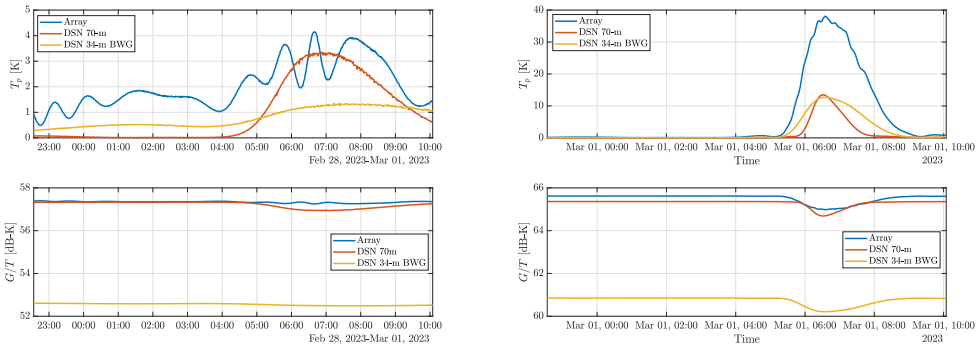

(a) X-band **(b) Ka-band**

Figure 8. Comparison of equivalent hot body noise temperature at X-band and Ka-band for Juno flyby.

Figure 8 provides the result of this analysis at both X- and Ka-band. It plots both the effective noise temperature "seen" by each system and the resulting G/T of the ground system (assuming no arraying losses). Several comments are noteworthy:

- The equivalent hot body noise temperature is one order of magnitude higher at Ka-band compared to X-band. This happens because the beam of the antenna (or array) is more directive, so Jupiter acts as a larger source of radiation.
- The G/T of the array at X-band is 1.3 dB lower than a DSN 70-m when hot body noise is not a factor. However, the performance of the array is superior to that of a 70-m antenna at Ka-band. This is driven by the assumption that a 70-m antenna has a 50% aperture efficiency at Ka-band.
- At X-band, the noise temperature "seen" by the array fluctuates by ∼2 K. This is due to the motion of the array grating in the local sky as the spacecraft is being tracked. Similar phenomena occurs at Ka-band, but its magnitude is dwarfed compared to the overall increase in noise temperature.
- Some curves (e.g., DSN 70-m at X-band) exhibit very fast fluctuations, especially when T_p is maximum. They are artifacts from the numerical integration process and thus should be discarded.

VI. Conclusions

This article provides an analytical model to quantify the effect of hot body noise on arrays of DSN antennas. It is shown that under narrowband operation, the effect of

the hot body can be simply accounted for as an effective noise temperature. Its value can be calculated by integrating the radiation pattern of the array over the body's blackbody temperature spatial distribution. For wideband operation, a similar result is derived with minor modifications that take into account the dependence of the body's radiation with frequency.

Using these results, we then define a metric to classify sources of hot body noise as extended or compact by comparing the angular extent of the hot body with the main beam of the array. In the case of extended sources, it is shown that significant amounts of blackbody radiation can be received by the array even if the main beam does not intersect with the planet. Indeed, because of the large spacing between DSN antennas compared to the wavelengths of operation, arraying them produces large grating lobes with small angular separation through which radiation is received.

Compact sources can be treated as point sources when their angular extent is very small compared to the main beam of the array. Therefore, the hot body noise effect will be significant only when the point source is located within the main beam, or within one of the adjacent grating lobes. When that is the case, the hot body acts as a source of perfectly correlated noise across all antennas in the array. As a result, the performance of the array becomes limited by hot body noise and cannot be improved even if the number of antennas increases.

Acknowledgments

The research was carried out at the Jet Propulsion Laboratory, California Institute of Technology, under a contract with the National Aeronautics and Space Administration (80NM0018D0004).

The author would like to acknowledge Marin Anderson, from the Jet Propulsion Laboratory, for her thoughtful comments and suggestions, as well as Kimberly Rizzo and Mary Young, also from the Jet Propulsion Laboratory, for their thorough editorial reviews.

References

[1] "Deep Space Network Services Catalog," Jet Propulsion Laboratory, Technical Report 820-100, Rev. H, June 2022.
https://deepspace.jpl.nasa.gov/files/820-100-H.pdf

[2] R. J. Dewey, "The Effects of Correlated Noise in Intra-Complex DSN Arrays for Galileo Telemetry Reception," The Interplanetary Network Progress Report, vol. 42-111, Jet Propulsion Laboratory, Pasadena, California, pp. 1–24, November 15, 1992.
https://ipnpr.jpl.nasa.gov/progress_report/42-111/111M.pdf

[3] S. J. Orfanidis, 2002, "Electromagnetic Waves and Antennas Volume 2".

[4] D. H. Rogstad, A. Mileant, and T. T. Pham, "Antenna Arraying Techniques in the Deep Space Network." Hoboken, NJ: Wiley, 2005.

[5] "Steradian," 2023. https://en.wikipedia.org/wiki/Steradian#Otherproperties

[6] Jet Propulsion Laboratory, "Atmospheric and Environmental Effects," Jet Propulsion Laboratory, Technical Report 810-005, 105, Rev. E, October 2015. https://deepspace.jpl.nasa.gov/dsndocs/810-005/105/105E.pdf

[7] A. Mileant and S. Hinedi, "Overview of Arraying Techniques in the Deep Space Network," The Interplanetary Network Progress Report, vol. 42-104, Jet Propulsion Laboratory, Pasadena, California, pp. 1–31, February 15, 1991. https://ipnpr.jpl.nasa.gov/progress_report/42-104/104K.pdf

[8] "Telemetry General Information," Jet Propulsion Laboratory, Technical Report 810-005, 206, Rev. E, October 2023. https://deepspace.jpl.nasa.gov/dsndocs/810-005/206/206E.pdf

APPENDIX

I. Distance Between DSN Stations

Table 1. Euclidean distances in kilometers between DSN stations.

		GDSCC			MDSCC						CDSCC			
		DSS-14	DSS-24	DSS-25	DSS-26	DSS-63	DSS-65	DSS-53	DSS-54	DSS-55	DSS-56	DSS-43	DSS-34	DSS-35	DSS-36
GDSCC	DSS-14	0	9.6	9.9	10.1	8390.4	8390.5	8390.4	8390.4	8390.6	8390.5	10589	10588.8	10588.8	10588.9
	DSS-24		0	0.3	0.5	8394.8	8394.8	8394.7	8394.7	8394.9	8394.8	10587.1	10586.9	10586.9	10587
	DSS-25			0	0.3	8394.9	8395	8394.9	8394.9	8395	8395	10587	10586.9	10586.8	10586.9
	DSS-26					8394.9	8395	8394.9	8394.9	8395	8395	10587.1	10586.9	10586.9	10587
MDSCC	DSS-63					0	0.5	0.6	0.8	0.9	0.7	12514.6	12514.6	12514.5	12514.5
	DSS-65						0	0.2	0.3	0.4	0.2	12514.6	12514.6	12514.6	12514.5
	DSS-53							0	0.2	0.3	0.2	12514.7	12514.6	12514.6	12514.6
	DSS-54								0	0.2	0.2	12514.7	12514.7	12514.6	12514.6
	DSS-55									0	0.2	12514.6	12514.6	12514.6	12514.5
	DSS-56										0	12514.6	12514.6	12514.6	12514.5
CDSCC	DSS-43											0	0.4	0.7	0.8
	DSS-34												0	0.3	0.5
	DSS-35													0	0.3
	DSS-36														0